Available online at www.sciencedirect.com
SCIENCE DIRECT®
Tectonophysics 370 (2003) 95–104
TECTONOPHYSICS
www.elsevier.com/locate/tecto

Microstructural control on the elastic properties of thermally cracked granite

T. Reuschlé*, S. Gbaguidi Haore, M. Darot

Institut de Physique du Globe de Strasbourg (CNRS/ULP), 5 rue René Descartes, 67084, Strasbourg Cedex, France

Accepted 31 March 2003

Abstract

Compressional waves velocity V_P was measured during long-term experiments in a high-pressure vessel (in the range [10–75] MPa for confining and pore pressures). Experiments were carried out on a granite specimen prepared by a controlled heating treatment at 510 °C, which generated thermal cracks.

Data analysis is proposed by using an effective medium approach based on Kachanov's [Appl. Mech. Rev. 45 (1992)304] model. The elastic behaviour of the cracked rock is controlled by the crack density parameter which varies with confining and pore pressures due to crack closure. In order to model the progressive closure of cracks, we assume elliptical cracks with major axis $2c$ and aspect ratio α. By using a conformal mapping technique, we derive the variation of the crack aspect ratio as a function of effective pressure, the effective pressure coefficient η depending on α and Poisson's ratio v_0. As a result, we compute the crack density parameter and the elastic moduli of the cracked rock as a function of confining and pore pressures. To take into account the heterogeneity of the rock sample, a peak-like distribution of crack aspect ratios is introduced, which allows us to calculate the acoustic velocity V_P for various effective pressures.

Comparison is made between theoretical and experimental values and shows that this simple model captures the essential features of the acoustic velocity variation: an increase of V_P when pore pressure is decreased followed by a plateau for a threshold pore pressure. Best consistency between theoretical and experimental velocity values is obtained by introducing a second crack population with a higher mean aspect ratio and an irreversible closure mechanism as effective pressure is cycled.

Keywords: Microcracks; Granite; Thermal cracking; Acoustic wave velocity; Effective medium

1. Introduction

The effect of thermal cracking on the physical properties of rocks is of great interest for various industrial applications like the optimisation of geothermal recovery, or the safe design of nuclear and toxic waste repositories, but it also applies to various natural processes like volcanism or metamorphism. It is important to see how modifications of the environmental stress state by man-induced activities or natural processes like tectonics may alter the rock structure thus leading to changes in physical properties of the host rock.

Rocks can be considered as a dual space composed of a "solid" space (i.e. the mineral matrix)

* Corresponding author. Tel.: +33-3-90-24-00-48; fax: +33-3-90-24-01-25.
E-mail address: Thierry.Reuschle@eost.u-strasbg.fr (T. Reuschlé).

0040-1951/03/$ - see front matter © 2003 Elsevier B.V. All rights reserved.
doi:10.1016/S0040-1951(03)00179-3

and a "void" space (the set of cracks and pores). Their physical properties are strongly dependent on the characteristics of the void space: pore/crack geometry, pore/crack density,... The description of microstructure is difficult and time-consuming but the data obtained are especially valuable for testing models. Actually, various theoretical models were developed to derive elastic properties from microstructural parameters (Bruner, 1976; Kachanov, 1992; Kemeny and Cook, 1986; O'Connell and Budiansky, 1974; Walsh, 1965). On the other hand, numerous experimental studies have been reported which demonstrate the influence of cracks on acoustic properties (Birch, 1960; Kern et al., 1997; Meglis et al., 1996; Todd and Simmons, 1972). For example, Todd and Simmons (1972) showed from acoustic waves velocity measurements as a function of pore pressure in low-porosity rocks that the velocity V_P is controlled by the effective pressure P_{eff} defined as $P_{eff}=P_C-\eta P_P$, where P_C is the confining pressure, P_P is the pore pressure and η is a coefficient smaller than unity. By using a simplified version of the acoustic wave propagation theory developed by Biot (1956a,b), Todd and Simmons (1972) wrote η as

$$\eta = 1 - \frac{(\partial V_P/\partial P_P)_{\Delta P}}{[\partial V_P/\partial(\Delta P)]_{P_P}} \quad (1)$$

where $(\partial V_P/\partial P_P)_{\Delta P}$ may be interpreted as a measure of the change in the compressional velocity of the individual grains of the rock with hydrostatic pore pressure at constant $\Delta P=P_C-P_P$, and $[\partial V_P/\partial(\Delta P)]_{P_P}$ is the change in the compressional velocity of the whole rock with a change in P_C-P_P at constant pore pressure.

The scope of this paper is to check the influence of pore/crack microstructure on the elastic properties of the rock. Our starting point is an intact rock sample that we subject to a thermal pretreatment to induce isotropic microcracking. Thermal cracking is due to internal stress concentrations following thermal expansion mismatch or thermal expansion anisotropy of grains. Fredrich and Wong (1986) examined the effects of temperature changes on the pore structure. They distinguished intergranular and intragranular cracks. Wang et al. (1989) investigated thermal cracking in four heated granites: they quantified thermally induced cracking. As thermal cracking affects pore microstructure, it can greatly influence transport properties: permeability (Darot and Reuschlé, 2000a) and electrical conductivity (Ruffet, 1993). In this paper, we will focus on acoustic velocity measurements as a function of both confining and pore pressures on a granite sample that was preheated at 510 °C.

Next, the experimental data will be analysed by an effective medium approach based on Kachanov's (1992) model. In this model, the elastic behaviour of the cracked rock is controlled by the crack density parameter that varies with confining and pore pressures by crack closure. To take into account the heterogeneity of the rock sample, a peak-like distribution of initial crack aspect ratio and a crack closing rule will be introduced, which will allow us to calculate the crack density parameter for various pressures. As a result, the theoretical acoustic velocities will be compared to the experimental data.

2. Experimental procedure and results

A granite core (20 mm in diameter and 40 mm in length) was drilled out of a single block of La Peyratte granite. This fine-grained granite (1.5 mm grain size) is extracted from a quarry near Poitiers (W France) (Turpault, 1989); it is composed of 40% plagioclase, 26% K-feldspar, 24% quartz and 10% biotite. Two parallel flat faces were machined halfway up for the location of the piezoceramics. A crack population was generated inside the specimen by a controlled heating treatment at 510 °C which ensured a porosity increase from 0.6% to 1.2% (Darot and Reuschlé, 2000b). When back to room temperature, the piezoceramic transducers were glued directly on the rock for a good mechanical coupling. The whole specimen equipped with its transducers was saturated under vacuum with deionized water and inserted in a jacket clamped on the end-pieces. Electric and hydraulic insulation was insured to avoid any leakage. Experiments were performed on the set-up described in Fig. 1. All the experimental parameters including the acoustic signal visualized on the oscilloscope, were digitized, recorded vs. time and saved on a computer.

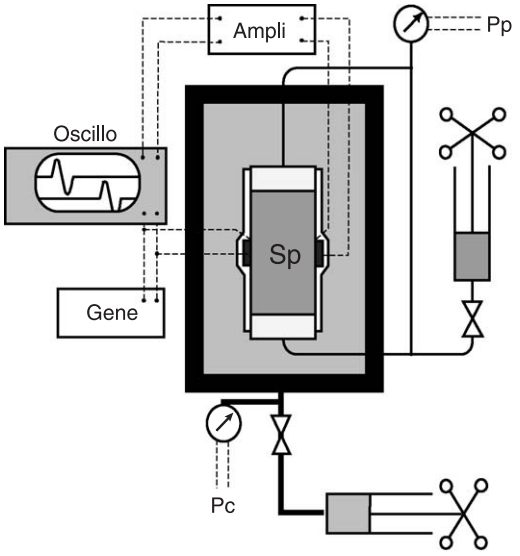

Fig. 1. The experimental setup. The specimen Sp equipped with piezoceramic transducers is insulated from the confining pressure P_C by a jacket clamped on end-pieces. The 100-MPa pressure cell and the confining pressure circuit are in heavy lines. The 100-MPa pore pressure circuit is in light lines. The V_P setup is composed of two piezoceramic transducers (700 kHz resonance frequency) connected to a generator, an amplifier and a two-channel digital oscilloscope.

P-wave velocity V_P was calculated using the transmission travel time of an acoustic pulse across the specimen between a transceiver and a receiver (both made of PZT piezoceramic with a resonant frequency of 700 kHz). The acoustic wave velocity measurement chain was composed of a generator giving the excitation to the transmitter, the receiver being connected to a 60-dB amplifier which allows the signal to be visualized on a two-channel oscilloscope. The travel time was measured directly on the oscilloscope screen with an accuracy of 10 ns which corresponds to a V_P accuracy better than ± 20 m/s.

The role of both pore and confining pressures on V_P was explored with pressure cycles experiments. A set of decreasing pore pressures was examined systematically for various increasing confining pressures. For each [P_C; P_P] couple, the P-wave travel time was determined as described above.

For the first step, P_C was risen to 2 MPa to insure jacket tightness onto the specimen. Then P_C and P_P were risen simultaneously up to, respectively, 10 and 8 MPa, keeping the differential pressure $P_C - P_P$ equal to 2 MPa. During the transient towards equilibrium, the acoustic signal from the receiver was recorded continuously and visualized on the oscilloscope screen until equilibrium was reached. At equilibrium, the P-wave travel time was determined and the signal recorded on a computer. This recording procedure was applied to successive decreasing P_P values. The pore pressure was then risen back step by step to the initial value. When equilibrium was reached, the confining pressure was increased to the next value with the differential pressure being kept constant and equal to 2 MPa. And a new cycle on P_P was started.

Water-filled cracks have been known for a long time to have a significant effect on V_P in a fractured rock (Johnston and Toksöz, 1980); our data in the 100-MPa confining pressure range confirm this important role of cracks on acoustic velocities. Raw data are shown in Fig. 2. For a constant confining pressure, V_P increases while pore pressure decreases; for a given pore pressure, V_P increases with increasing confining pressure. The general V_P vs. P_P trend can be described as a two-step process: first, a progressive quasi-linear increase as P_P decreases, and second, a quasi-constant velocity regime. A kink on almost all curves indicates the transition between these two types of responses.

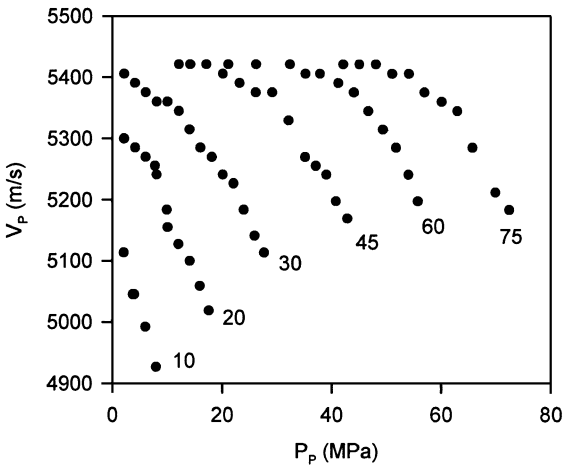

Fig. 2. Acoustic waves velocity V_P vs. pore pressure P_P for different constant confining pressures P_C (labelled in MPa near the end of each curve).

3. Theoretical analysis and discussion

At a given confining pressure, decreasing pore pressure induces forces which tend to bring facing crack surfaces closer. This induces changes in the microstructural geometry thus affecting the acoustic waves velocity. Numerous models have been developed to relate changes in microstructural parameters to acoustic waves propagation properties (Berge et al., 1992; Henyey and Pomphrey, 1982; Le Ravalec and Guéguen, 1996). These models are mainly based on the concept of equivalent effective medium, that is a homogeneous medium which has the same elastic properties as the real heterogeneous cracked rock. One hypothesis of this approach is that the crack centres have to be randomly distributed, that is the medium has to be statistically homogeneous. Another hypothesis is that the cracks are isolated objects not interacting with the others. This point has been discussed in detail by Kachanov (1992). Consider that locations of crack centres are random. One may expect that the competing effects of shielding and amplification are balanced and cancel each other, i.e., that the randomness of crack centres ensures the absence of "bias" toward either amplifying or shielding configurations. If this is indeed so, then the approximation of noninteracting cracks remains accurate at high crack densities, in spite of strong interactions. Kachanov (1994) has shown that, for at least two orientational statistics—parallel and randomly oriented cracks—these expectations are confirmed by computer experiments and calculations of the method of effective field. We have also made a third hypothesis, which is the isotropy of the rock. This has been checked by measuring V_P in three perpendicular directions: the velocity variations are within 2%. Once these assumptions are made, the only microstructural parameter that has to be introduced in the models is the crack density parameter. The basic concept of the effective medium approach is that the presence of a crack disturbs the deformation field in the intact rock subjected to an external stress field. One can thus compute the variations of the elastic moduli of the rock as a function of the crack density parameter χ and the elastic moduli of the intact rock, that is Young's modulus E_0 and Poisson's coefficient v_0.

We consider flat spheroidal "penny-shape" cracks of initial radius c_0 and width b_0 ($b_0 \ll c_0$), which leads to a shape factor $\alpha_0 = b_0/c_0$. Since we measured acoustic waves velocity in a saturated sample, we have to take into account the compressibility β of the fluid phase. This is done by introducing a parameter δ defined by:

$$\delta = \frac{3\pi\beta E_0 \alpha_0}{16(1 - v_0^2)} \tag{2}$$

where $\beta = 2.3\ \mathrm{GPa}^{-1}$ for water.

The elastic moduli E and v of the cracked rock are then given by (Kachanov, 1992):

$$\left(\frac{E}{E_0}\right)^{-1} = 1 + \chi \frac{16(1 - v_0^2)}{9(1 - v_0/2)} \times \left\{1 - \frac{3}{5}\left[1 - \left(1 - \frac{v_0}{2}\right)\frac{\delta}{1 + \delta}\right]\right\}$$

$$\frac{v}{v_0} = \frac{E}{E_0}\left[1 + \frac{8(1 - v_0^2)}{45(1 - v_0/2)}\chi\right] \tag{3}$$

Once the elastic moduli are computed, it is easy to derive the P-wave velocity V_P using the following equation:

$$V_P = \sqrt{\frac{(1 - v)E}{(1 + v)(1 - 2v)\rho}} \tag{4}$$

where ρ is the density of the rock.

The crack density parameter χ was introduced by Walsh (1965) and is defined as:

$$\chi = \frac{1}{V}\sum_i c_i^3 \tag{5}$$

where the sum runs over all cracks of the rock sample. Since the rock has a fairly uniform grain size, we may assume that all cracks have the same radius c, Eq. (5) can be simplified to $\chi = Nc^3$, where N is the number of cracks per unit volume of rock.

For a given confining pressure, when the pore pressure is decreased, cracks start to close. Depending on their initial aspect ratio α_0, there exists a critical pore pressure for which some cracks are completely closed, thus decreasing N and χ. Therefore, we have to develop an evolution rule for the

aspect ratio α as a function of pressures P_C and P_P. Mavko and Nur (1978) have developed a calculation scheme of crack deformation under hydrostatic pressure that Doyen (1987) applied to saturated cracked rocks. In this approach, the crack aspect ratio α is shown to decrease linearly as differential pressure $P_C - P_P$ is increased. However, previous experimental studies on various rocks have shown that confining and pore pressures do not have a symmetrical effect on physical properties. Indeed, the pressure controlling these properties is the effective pressure $P_C - \eta P_P$, where the effective pressure coefficient η is usually lower than unity. For example, Bernabé (1987) has found η values ranging between 0.5 and 1 for permeability measurements run on low-permeability sandstone and granite. For La Peyratte granite, Darot and Reuschlé (2000a) obtained η values ranging between 0.7 and 1 for permeability and acoustic waves velocity measurements. As pointed out by Bernabé (1988), the effective pressure coefficient may be stress-path dependent. During confining and pore pressures cycles, the coefficient η was shown to vary depending on which pressure was first modified. However, this dependency on stress path decreased rapidly with the number of cycles. Effective pressure coefficient η may also vary with confining pressure. As shown by Bernabé (1986) on Chelmsford granite and Barre granite, η slightly decreases with increasing confining pressure. This has been interpreted in terms of changes in the geometry of the cracks during closure.

In order to constrain our evolution rule for cracks we use the following approximation: the penny-shape crack is replaced by a cylindrical tube with elliptical cross section, where c_0 is the semi-major axis and b_0 is the semi-minor axis of the ellipse. This crack is treated as a two-dimensional void inclusion in plane strain embedded in a solid, homogeneous and isotropic elastic matrix. The stresses acting on the cavity are the confining and pore pressures P_C and P_P. Using a conformal mapping technique (Muskhelishvili, 1977), we can calculate the normal displacement at the crack surface. In the minor axis direction, this displacement U is written as:

$$U = \frac{2c(1-\nu_0^2)}{E_0}(P_C - \eta P_P) \tag{6}$$

where the effective pressure coefficient η is given by:

$$\eta = \frac{1 + (1-\alpha)(1-2\nu_0)}{2(1-\nu_0)} \tag{7}$$

In Fig. 3, we have reported the variations of η as a function of α, the shape factor ranging from 0 (flat crack) to 1 (circular tube). We see in this figure that for crack aspect ratio usually found in granite ($\alpha < 0.01$) the effective pressure coefficient is very close to 1. An interpretation of the decrease of α with increasing confining pressure P_C has been given by Bernabé (1986): the cracks in the rocks are supposed to have rough walls; during closure, when asperities come into contact, a low aspect ratio crack is progressively transformed into an array of smaller cracks with higher aspect ratio (Walsh and Grosenbaugh, 1979) and therefore lower α (Fig. 3). In the following, we do not consider this crack evolution scheme and we assume that there are no asperities on the crack surfaces.

Introducing the effective pressure $P_{eff} = P_C - \eta P_P$, we can compute the stressed crack half-width $b = b_0 - U$, and we derive the evolution rule for crack aspect ratio α as a function of P_{eff} from Eq. (6):

$$\alpha = \alpha_0 - \frac{2(1-\nu_0^2)}{E_0} P_{eff} \tag{8}$$

The critical effective pressure for crack closure is then easily computed from Eq. (8) by taking $\alpha = 0$. Eq.

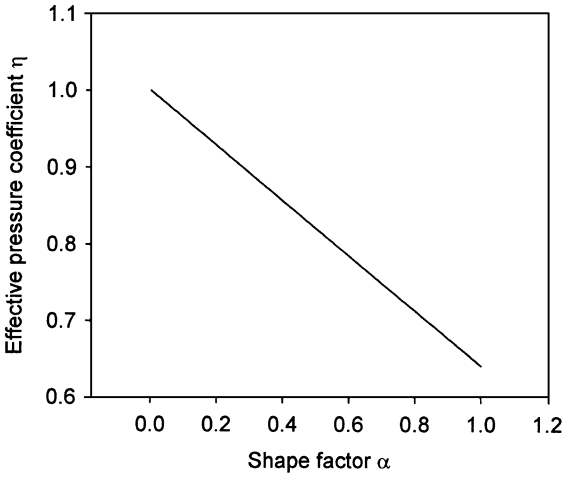

Fig. 3. Effective pressure coefficient η vs. crack aspect ratio α. Poisson's coefficient ν_0 has been taken equal to 0.22.

(8) shows that the critical aspect ratio is increasing with pressure. Combining this result and the experimental velocity data presented in Fig. 2 gives some information about the shape factor range of the cracks present in the rock sample. At high velocity or effective pressure, the observed plateau regime corresponds to the closure of cracks with maximum aspect ratio. By taking $\eta = 1$, the beginning of the plateau corresponds to a critical effective pressure of about 32 MPa. Young's modulus E_0 and Poisson's coefficient v_0 for the intact granite were determined from strain measurements during a uniaxial compression test on a nontreated sample. We found $E_0 = 75$ GPa and $v_0 = 0.22$. These static elastic constants compare well with the Voight–Reuss–Hill average given by David et al. (1999) and deduced from the mineralogical composition of La Peyratte granite. Introducing these values in Eq. (8) leads to $\alpha \approx 8.10^{-4}$. Using a similar calculation, the lowest measured V_P at $P_C = 10$ MPa and $P_P = 8$ MPa corresponds to an aspect ratio of about 5.10^{-5}. It implies that there exist cracks with aspect ratios down to a minimum threshold smaller than this value. Since V_P is increasing with P_{eff}, it means that cracks have aspect ratios ranging between these two values and that they successively close as P_{eff} is increased. To take into account this heterogeneity of crack microstructure, we have to introduce a distribution of crack aspect ratios. Following the approach proposed by David et al. (1990), we use a peak-like distribution controlled by five parameters: the minimum aspect ratio α_{min}, the maximum aspect ratio α_{max}, the central aspect ratio α_c and the two decreasing factors d_1 and d_2 (Fig. 4). The probability distribution function $f(\alpha)$ of crack aspect ratio is then given by:

$$f(\alpha) = a_1 \exp(b_1 \alpha) W(\alpha_{min}, \alpha_c) + a_2 \exp(-b_2 \alpha) W(\alpha_c, \alpha_{max}) \quad (9)$$

$W(\alpha_i, \alpha_j)$ is the rectangular unity window on the interval $[\alpha_i, \alpha_j]$ and is defined by $W(\alpha_i, \alpha_j) = H(\alpha - \alpha_i) - H(\alpha - \alpha_j)$, where $H()$ is the Heaviside distribution. The parameters a_1, a_2, b_1 and b_2 are inferred from the five controlling parameters of the distribution defined above. Microstructural data compiled by Brace (1977) show that Eq. (9) may apply for various granites. We then assume this equation is also a good description of the crack shape factor distribution in the La Peyratte granite. Estimate for

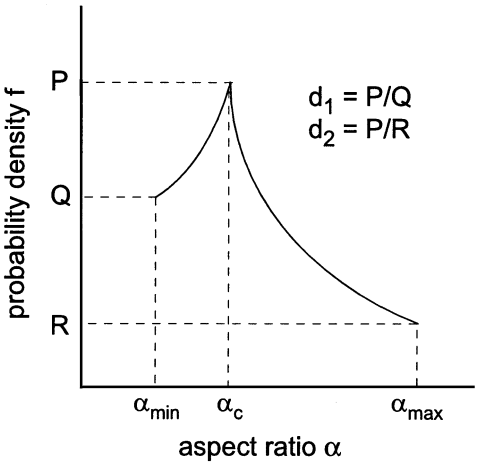

Fig. 4. Probability distribution function $f(\alpha)$ of aspect ratio α. The definition of the controlling parameters α_{min}, α_c, α_{max}, d_1 and d_2 is given in the figure.

α_{max} has been deduced from the high velocity plateau regime on Fig. 2, that is $\alpha_{max} = 8.10^{-4}$. An estimate for α_c may be deduced from the first V_P measurement in our (P_C, P_P) cycles, 'leading to $\alpha_c = 5.10^{-5}$. For simplicity, we assume that the decreasing factors d_1 and d_2 are equal. The two last parameters, α_{min} and $d = d_1 = d_2$, are then determined by fitting the experimental velocity data with the theoretical values obtained at $P_C = 10$ MPa.

In order to compute V_P for a given P_P, we need to know the initial value of the crack density parameter χ_0. This is achieved by introducing the porosity of the rock sample. Porosity ϕ has been found equal to 1.2% for the La Peyratte sample heated at 510 °C. The volume of a single penny-shape crack is $V_{crack} = \pi c^3 \alpha$. Introducing this crack volume and porosity ϕ into Eq. (5), and assuming that all cracks have the same radius, we obtain the following relation between the initial crack density parameter χ_0 and porosity ϕ:

$$\chi_0 = \frac{3\phi}{4\pi\bar{\alpha}} \quad (10)$$

where $\bar{\alpha}$ is the mean aspect ratio of the crack population given by:

$$\bar{\alpha} = \int_{\alpha_{min}}^{\alpha_{max}} \alpha f(\alpha) d\alpha \quad (11)$$

Starting at $P_P = 8$ MPa, we are now able to describe the evolution of velocity V_P as P_P is decreased. For a given P_P value, we calculate the effective pressure coefficient η as a function of aspect ratio α by using Eq. (7). Eq. (8) allows the computation of the critical aspect ratio α_{clo}, the minimum α value of the remaining open cracks at given P_P. The number of cracks per unit volume of rock still open at P_P is then given by:

$$N = N_0 \int_{\alpha_{clo}}^{\alpha_{max}} f(\alpha)\mathrm{d}\alpha \tag{12}$$

where N_0, the initial number of cracks per unit volume of rock, is given by $N_0 = \chi_0/c^3$.

Introducing N in Eq. (5) leads to the crack density parameter χ at P_P, which no longer depends on c. It is thus straightforward to compute V_P by using Eqs. (3) and (4), where δ is derived from Eq. (2) by averaging over all remaining open cracks:

$$\delta = \frac{3\pi\beta E_0}{16(1-\nu_0^2)} \int_{\alpha_{clo}}^{\alpha_{max}} \alpha f(\alpha)\mathrm{d}\alpha \tag{13}$$

The same calculation is done for the different experimental P_C values and we can compare the various theoretical V_P evolutions to the experimental ones. The first point we have to check is the consistency between both theoretical and experimental initial V_P values at lowest P_C and P_{eff}. Because V_P is decreasing as χ increases, an overestimation of the initial velocity can be obtained by replacing $\bar{\alpha}$ by α_{max} in Eq. (10). This operation leads to an initial $V_P \approx 2800$ m/s much lower than the experimental value (4930 m/s). Since porosity ϕ has been measured independently, it means that the mean aspect ratio $\bar{\alpha}$ we have to introduce in Eq. (10) must be higher than α_{max}. This may be explained by the existence of two crack populations: a first one consisting of cracks with shape factors in the range $[\alpha_{min}, \alpha_{max}]$ which are progressively closed during our experiments up to 35 MPa effective pressure, and a second population of cracks with aspect ratios higher than α_{max} which cannot be closed in the effective pressure range we explored during our experiments. This second crack family would thus not affect the velocity V_P evolution up to 35 MPa effective pressure. However, by introducing the same closure mechanism as above, their higher shape factors would explain the effective pressure dependence of V_P usually observed in crystalline or metamorphic rocks up to about 400 MPa (Birch, 1960; Kern et al., 1997; Kern and Tubia, 1993; Nur and Simmons, 1969). In fact, this kind of double crack porosity is similar to the one introduced by Le Ravalec et al. (1996) to analyse the effect of fluid saturation on acoustic velocities in rocks.

We have no direct control on the properties of the second crack population. Nevertheless, fitting the initial experimental velocity to the theoretical one gives some constraint on the relative volume occupied by these cracks. Furthermore, the high velocity plateau regime gives a lower limit to the shape factors of the cracks belonging to the second family, that is $\alpha \geq 8.10^{-4}$. To simplify our analysis, we suppose that this second family is composed of cracks having a mean crack shape α_2. Let ϕ_1 and ϕ_2 be the porosity occupied by the crack populations 1 and 2, respectively. Assuming that all cracks have the same radius, the initial number of cracks N_{10} and N_{20} belonging to families 1 and 2 are given by:

$$N_{10} = \frac{3\phi_1}{4\pi\bar{\alpha}_1 c^3} \quad N_{20} = \frac{3\phi_2}{4\pi\bar{\alpha}_2 c^3} \tag{14}$$

where $\bar{\alpha}_1$ is the mean aspect ratio of crack family 1 derived from Eq. (11). The number N of cracks per unit volume of rock still open at a given P_P is derived from the following equation similar to Eq. (12):

$$N = N_{10} \int_{\alpha_{clo}}^{\alpha_{max}} f(\alpha)\mathrm{d}\alpha + N_{20} \tag{15}$$

The calculation of parameter δ has to be changed to take into account the second crack population. This is simply done by introducing the mean crack shape $\bar{\alpha}_2$ of crack family 2 into Eq. (13), which leads to:

$$\delta = \frac{3\pi\beta E_0}{16(1-\nu_0^2)} \left(\frac{N_1}{N} \int_{\alpha_{clo}}^{\alpha_{max}} \alpha f(\alpha)\mathrm{d}\alpha + \frac{N_{20}}{N}\bar{\alpha}_2 \right) \tag{16}$$

where N_1 is the number of cracks of family 1 still open at pressure P_P. The crack density parameter χ at a given P_P is deduced from Eq. (5): $\chi = Nc^3$. Acoustic waves velocity V_P is then given by Eqs. (3) and (4) where crack density parameter χ is changing with P_C and P_P.

In Fig. 5, we show the comparison between the experimental velocity data and the theoretical values deduced from our model. The microstructural param-

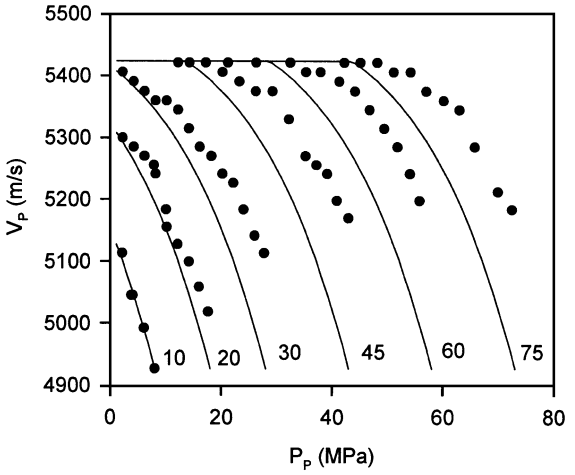

Fig. 5. Comparison between the experimental velocity data and the theoretical values deduced from the model. The aspect ratio distribution parameters of the first crack family, the mean aspect ratio of the second crack family and the porosity occupied by each crack family are given in Table 1. The confining pressure value is labelled in MPa near the end of each curve.

eters were determined by best fitting the velocity curve obtained at $P_C = 10$ MPa, which corresponds to the first pressure cycle in our experiments. They are summarized in Table 1. We see in Fig. 5 that the general trend observed experimentally is rather well described by our model: an increase of velocity V_P with effective pressure followed by a plateau regime. However, two features cannot be reproduced by the model: the change in slope of the V_P vs. P_P evolution as confining pressure is increased, and the increase with confining pressure of the velocity measured at lowest effective pressure. One can also notice an increasing difference between the theoretical and experimental V_P evolutions as confining pressure is increased. A possible explanation for the increase of the low effective pressure velocity may be the irreversible closure of a subset of the first crack population when effective pressure is cycled.

Table 1
Aspect ratio distribution parameters of the first crack family, mean aspect ratio of the second crack family and porosity occupied by each crack family

α_{min}	α_c	α_{max}	d_1	d_2	$\bar{\alpha}_2$	ϕ_1	ϕ_2
1.10^{-6}	5.10^{-5}	8.10^{-4}	10	10	$4.8{\cdot}10^{-2}$	0.03%	1.17%

We propose to model this irreversible closure by introducing ϕ_{1res}, the residual porosity occupied by the cracks belonging to the first family and still open at the start of a pore pressure cycle at constant P_C. Since there is no simple way to model the control of the aspect ratio on the irreversible crack closure, we assume that this mechanism affects the cracks of the first population independently of their aspect ratio. Hence, it follows that the initial number N_{10} of cracks belonging to family 1 has to be changed to:

$$N_{10} = \frac{3\phi_{1res}}{4\pi\bar{\alpha}_1 c^3} \tag{17}$$

where $\bar{\alpha}_1$ is still derived from Eq. (11). Introducing Eq. (17) into Eqs. (15) and (5) leads to the crack density parameter χ and hence to velocity V_P. The parameter ϕ_{1res} is determined by using the velocities measured at lowest effective pressure for each P_C value.

Fig. 6 summarizes the variation with confining pressure of the residual porosity ϕ_{1res} which ensures the best fit to the initial velocity data. Fig. 7 illustrates the comparison between the experimental velocity data and the theoretical values deduced from our model when an irreversible closure of cracks is introduced. We notice that the modified model is now able to capture all essential features of the experimental curves: the slope of the V_P vs. P_P curve

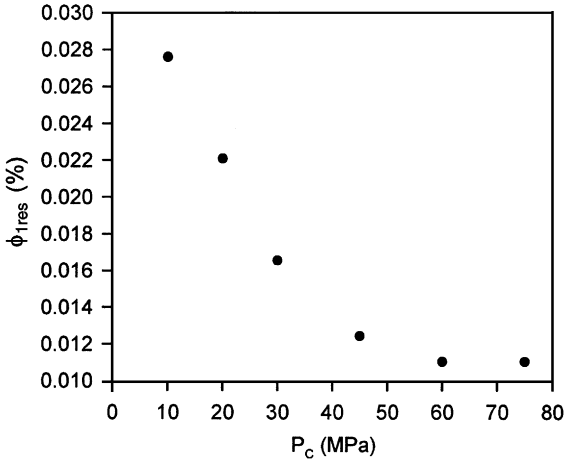

Fig. 6. Evolution of the residual porosity ϕ_{1res} occupied by the first crack population when an irreversible closure mechanism is introduced as effective pressure is cycled.

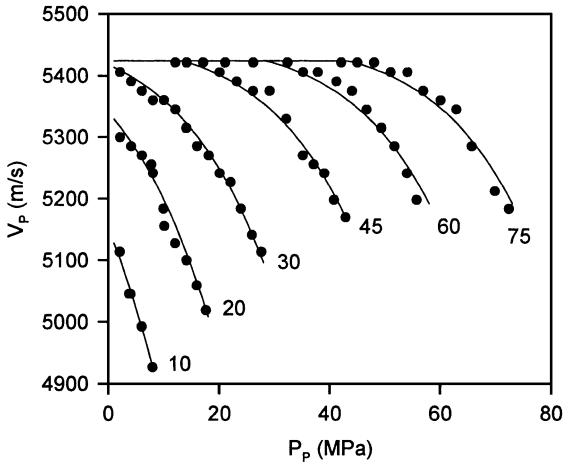

Fig. 7. Comparison between the experimental velocity data and the theoretical values deduced from the model when an irreversible closure mechanism is introduced. The microstructural parameters are the same as for Fig. 5. The residual porosity is given in Fig. 6. The confining pressure value is labelled in MPa near the end of each curve.

is now decreasing as P_C is increased, the increasing difference between theory and experiment observed in Fig. 5 has been reduced and the theoretical data are now quite consistent with the experimental values. This improved consistency is a strong support for our hypothesis of partial irreversible closure of cracks during pressure cycling.

4. Conclusion

The comparison between theoretical acoustic velocity values and experimental data illustrates the influence of crack microstructure evolution on the elastic properties of a rock. The crack content evolution was controlled during experiments by varying both confining and pore pressures. A data analysis based on the effective medium approach proposed by Kachanov (1994) has shown that this control operates through the crack density parameter χ which varies with confining and pore pressures by crack closure. When assuming reversible crack closure during pressure cycling, our analysis is able to capture the general trend of velocity evolution with pore pressure: an increase followed by a plateau at high effective pressure. This implies the existence of two crack families: a first one with aspect ratios following a peak-like distribution which is progressively closed during our experiments; a second one with a higher mean aspect ratio which is not affected by the pressure cycles. The remaining inconsistency between theory and experiments can be removed by introducing an irreversible closure mechanism as effective pressure is cycled.

This paper shows that our experimental data combined with a detailed analysis give some information on the microstructural parameters of the tested rock and their evolution with pressure. The next step of our approach will be to apply the same analysis to velocity data obtained in the same pressure conditions on La Peyratte granite samples prepared by a controlled heating at various temperatures. We will then be able to check the effect of thermal treatment on the evolution with pressure of the microstructural parameters. A further step will be to develop an analogous analysis for permeability data that were acquired in parallel with velocity measurements, to check whether the microstructural control is similar for both properties.

Acknowledgements

This is EOST contribution No. 2002.09-UMR7516. We are grateful to two anonymous reviewers for their helpful comments on the manuscript. The authors also thank Jean-Daniel Bernard for technical support during the course of this work.

References

Berge, P.A., Fryer, G.J., Wilkens, R.H., 1992. Velocity–porosity relationships in the upper oceanic crust: theoretical considerations. J. Geophys. Res. 97, 15239–15254.

Bernabé, Y., 1986. The effective pressure law for permeability in Chelmsford granite and Barre granite. Int. J. Rock Mech. Min. Sci. Geomech. Abstr. 23, 267–275.

Bernabé, Y., 1987. The effective pressure law for permeability during pore pressure and confining pressure cycling of several crystalline rocks. J. Geophys. Res. 92, 649–657.

Bernabé, Y., 1988. Comparison of the effective pressure law for permeability and resistivity formation factor in Chelmsford granite. Pure Appl. Geophys. 127, 607–625.

Biot, M.A., 1956a. Theory of propagation of elastic waves in a fluid-saturated porous solid-I. Low-frequency range. J. Acoust. Soc. Am. 28, 168–178.

Biot, M.A., 1956b. Theory of propagation of elastic waves in

a fluid-saturated porous solid-II. Higher frequency range. J. Acoust. Soc. Am. 28, 179–191.
Birch, F., 1960. The velocity of compressional waves in rocks to 10 kilobars, Part 1. J. Geophys. Res. 65, 1083–1102.
Brace, W.F., 1977. Permeability from resistivity and pore shape. J. Geophys. Res. 82, 3343–3349.
Bruner, W.M., 1976. Comment on 'Seismic velocities in dry and saturated cracked solids' by R.J. O'Connell and B. Budiansky. J. Geophys. Res. 81, 2573–2576.
Darot, M., Reuschlé, T., 2000a. Acoustic wave velocity and permeability evolution during pressure cycles on a thermally cracked granite. Int. J. Rock Mech. Min. Sci. 37, 1019–1026.
Darot, M., Reuschlé, T., 2000b. Effect of pore and confining pressures on V_P in thermally pre-cracked granites. Geophys. Res. Lett. 27, 1057–1060.
David, C., Guéguen, Y., Pampoukis, G., 1990. Effective medium theory and network theory applied to the transport properties of rock. J. Geophys. Res. 95, 6993–7005.
David, C., Menéndez, B., Darot, M., 1999. Influence of stress-induced and thermal cracking on physical properties and microstructure of La Peyratte granite. Int. J. Rock Mech. Min. Sci. 36, 433–448.
Doyen, P.M., 1987. Crack geometry in igneous rocks: a maximum entropy inversion of elastic and transport properties. J. Geophys. Res. 92, 8169–8181.
Fredrich, J.T., Wong, T.-F., 1986. Micromechanics of thermally induced cracking in three crustal rocks. J. Geophys. Res. 91, 12743–12764.
Henyey, F.S., Pomphrey, N., 1982. Self-consistent elastic moduli of a cracked solid. Geophys. Res. Lett. 9, 903–906.
Johnston, D.H., Toksöz, M.N., 1980. Ultrasonic *P* and *S* wave attenuation in dry and saturated rocks under pressure. J. Geophys. Res. 85, 925–936.
Kachanov, M., 1992. Effective elastic properties of cracked solids: critical review of some basic concepts. Appl. Mech. Rev. 45, 304–335.
Kachanov, M., 1994. Elastic solids with many cracks and related problems. Adv. Appl. Mech. 30, 259–445.
Kemeny, J., Cook, N.G.W., 1986. Effective moduli, non-linear deformation and strength of a cracked elastic solid. Int. J. Rock Mech. Min. Sci. Geomech. Abstr. 23, 107–118.
Kern, H., Tubia, J.M., 1993. Pressure and temperature dependence of *P*- and *S*-wave velocities, seismic anisotropy and density of sheared rocks from the Sierra Alpujata massif (Ronda peridotites, Southern Spain). Earth Planet. Sci. Lett. 119, 191–205.
Kern, H., Liu, B., Popp, T., 1997. Relationship between anisotropy of *P* and *S* wave velocities and anisotropy of attenuation in serpentinite and amphibolite. J. Geophys. Res. 102, 3051–3065.
Le Ravalec, M., Guéguen, Y., 1996. High- and low-frequency elastic moduli for a saturated porous/cracked rock-Differential self-consistent and poroelastic theories. Geophysics 61, 1080–1094.
Le Ravalec, M., Guéguen, Y., Chelidze, T., 1996. Elastic wave velocities in partially saturated rocks: saturation hysteresis. J. Geophys. Res. 101, 837–844.
Mavko, G.M., Nur, A., 1978. The effect of nonelliptical cracks on the compressibility of rocks. J. Geophys. Res. 83, 4459–4468.
Meglis, I.L., Greenfield, R.J., Engelder, T., Graham, E.K., 1996. Pressure dependence of velocity and attenuation and its relationship to crack closure in crystalline rocks. J. Geophys. Res. 101, 17523–17533.
Muskhelishvili, N.I., 1977. Some Basic Problems of the Mathematical Theory of Elasticity. Noordhoff International Publishing, Leyden. 732 pp.
Nur, A., Simmons, G., 1969. The effect of saturation on velocity in low porosity rocks. Earth Planet. Sci. Lett. 7, 183–193.
O'Connell, R.J., Budiansky, B., 1974. Seismic velocities in dry and saturated cracked solids. J. Geophys. Res. 79, 5412–5426.
Ruffet, C., 1993. La conductivité électrique complexe dans quelques roches crustales. PhD. Thesis, Université Louis Pasteur, Strasbourg.
Todd, T., Simmons, G., 1972. Effect of pore pressure on the velocity of compressional waves in low-porosity rocks. J. Geophys. Res. 77, 3731–3743.
Turpault, M.-P., 1989. Etude des mécanismes des altérations hydrothermales dans les granites fissurés. PhD. Thesis, Université de Poitiers.
Walsh, J.B., 1965. The effect of cracks on the compressibility of rock. J. Geophys. Res. 70, 381–389.
Walsh, J.B., Grosenbaugh, M.A., 1979. A new model for analyzing the effect of fractures on compressibility. J. Geophys. Res. 84, 3532–3536.
Wang, H.F., Bonner, B.P., Carlson, S.R., Kowallis, B.J., Heard, H.C., 1989. Thermal stress cracking in granite. J. Geophys. Res. 94, 1745–1758.